The Journal of Chemical Physics

Formation of hot ice caused by carbon nanobrushes. II. Dependency on the radius of nanotubes

Cite as: J. Chem. Phys. **154**, 094502 (2021); https://doi.org/10.1063/5.0044300
Submitted: 15 January 2021 . Accepted: 11 February 2021 . Published Online: 01 March 2021

Masakazu Matsumoto, Takuma Yagasaki, and Hideki Tanaka

The Journal of Chemical Physics ARTICLE scitation.org/journal/jcp

Formation of hot ice caused by carbon nanobrushes. II. Dependency on the radius of nanotubes

Cite as: J. Chem. Phys. 154, 094502 (2021); doi: 10.1063/5.0044300
Submitted: 15 January 2021 • Accepted: 11 February 2021 •
Published Online: 1 March 2021

Masakazu Matsumoto,[1,a)] Takuma Yagasaki,[2] and Hideki Tanaka[1]

AFFILIATIONS

[1] Research Institute for Interdisciplinary Science, Okayama University, Okayama 700-8530, Japan
[2] Division of Chemical Engineering, Graduate School of Engineering Science, Osaka University, Osaka 560-8531, Japan

Note: This paper is part of the JCP Special Topic on Fluids in Nanopores.
[a)] **Author to whom correspondence should be addressed:** vitroid@gmail.com

ABSTRACT

Stable crystalline structures of confined water can be different from bulk ice. In Paper I [T. Yagasaki *et al.*, J. Chem. Phys. **151**, 064702 (2019)] of this study, it was shown, using molecular dynamics (MD) simulations, that a zeolite-like ice structure forms in nanobrushes consisting of (6,6) carbon nanotubes (CNTs) when the CNTs are located in a triangle arrangement. The melting temperature of the zeolite-like ice structure is much higher than the melting temperature of ice I_h when the distance between the surfaces of CNTs is ~0.94 nm, which is the best spacing for the bilayer structure of water. In this paper, we perform MD simulations of nanobrushes of CNTs that are different from (6,6) CNTs in radius. Several new porous ice structures form spontaneously in the MD simulations. A stable porous ice forms when the radius of its cavities matches the radius of the CNTs well. All cylindrical porous ice structures found in this study can be decomposed into a small number of structural blocks. We provide a new protocol to classify cylindrical porous ice crystals on the basis of this decomposition.

INTRODUCTION

Water is a universal solvent in which a variety of substances dissolve, and many functions of biomolecules owe to this property of water.[1] The solubility of a solute in liquid water is dominated by the electrostatic interaction between the solute and water molecules. Gas molecules are almost insoluble in water due to the weak electrostatic interactions. The solubility of molecules in solid water is governed by a different rule. Water molecules can form porous but stable crystalline structures that are different from ice I_h in the presence of small hydrophobic molecules at low temperatures.[2] Although the attractive interactions between hydrophobic gas molecules and water molecules are weak, the solubility of the gas molecules in the resultant crystal, i.e., clathrate hydrate, is fairly high. The decomposition temperature of clathrate hydrate can be controlled by the choice of guest molecule and the partial pressure.[3] Therefore, clathrate hydrate can be used for various applications such as gas separation, fresh water production, and heat storage.[4,5]

Vacuum degassing of clathrate hydrate is a novel way to produce ice phases that are less dense than ice I_h.[6,7] Two ice phases, XVI and XVII, were synthesized using this method. Many other stable low-density ice phases have been proposed by computer simulation studies.[8–12] Ice ITT having channel-like cavities is one of them.[13] It was suggested that the ITT ice structure can be stabilized by filling the cavities with some guest molecules. Yagasaki *et al.* performed molecular dynamics (MD) simulations of carbon nanobrushes consisting of carbon nanotubes (CNTs) designed to fit the cavity of the ITT structure.[14] It was found that water molecules penetrate into a space between CNTs and form a crystal structure that is similar to, but different from, the ITT structure. The melting point of this new ice can be controlled by the length of the CNTs and the distance between the CNTs in the brush. The maximum melting temperature is higher than the melting temperature of ice I_h of the employed

force field model by 50 K. The obtained structure can be considered as a clathrate hydrate of the nanobrush, and it might be industrially useful if realized experimentally.

Only the CNT with a chiral index of (6,6) was considered in the previous study. In this paper, we perform MD simulations of nanobrushes of smaller and larger CNTs and find several new nanobrush clathrate hydrates. The structures and the melting temperatures of them are investigated.

METHODS

MD simulations are carried out using GROMACS 4.6.[15] The initial setup of the system is shown in Fig. 1. There are four regions in a rectangular simulation cell: vacuum, liquid water, nanobrush, and liquid water. Four uncapped CNTs are aligned parallel to the z-axis in the nanobrush region. The CNTs are fixed in the simulation cell so that they form a regular triangular lattice on the xy plane, and the space between the CNTs is filled with water molecules. The gap between the CNTs (the distance between the centers of the nanotubes minus the diameter of the nanotubes) is 0.94 nm, at which the melting temperature is maximized for (6,6) CNT brush.[14] This spacing is optimal to accommodate the bilayer structure of water. Barostats are not used in the MD simulations to keep the gap distance. The vacuum region ensures that the pressure of the entire system is maintained at the vapor pressure of water at the given temperature. The length of the nanotubes is fixed to 6 nm. The C–C bond length of the carbon nanotubes is 0.144 nm, and the terminal carbon atoms of the CNTs are modified with hydrogen atoms. The intermolecular Lennard–Jones (LJ) and intramolecular (bond, angle, and dihedral) parameters of CNT are taken from the OPLS-AA (optimized potentials for liquid simulations all-atom) model.[16,17] The standard geometric mean rule is used for unlike pair interactions.

Simulations are also performed for nanobrushes where CNTs are located in a square lattice arrangement, but no crystallization is observed in the temperature range we examine. Therefore, only the simulation results of the triangular arrangement are presented in this paper.

The structure and radius of a CNT is characterized by the chiral index.[18] The CNTs examined in this study are armchair CNTs with chiral indices from (2,2) to (16,16) corresponding a range of the CNT radius from 0.14 nm to 2.2 nm and zigzag CNTs with chiral indices from (3,0) to (19,0) corresponding a range of the radius from 0.12 nm to 1.51 nm. Note that the experimentally smallest CNT is (2,2).[19]

The TIP4P/2005 water model is used for the water–water interaction.[20] The melting point of this force field model is 250 K at 1 bar. The simulation time is 100 ns, during which we observe whether water in the nanobrush region freezes or not. We calculate the following quantity for each water molecule in the brush region for the last 10 ns of the simulation:

$$\delta_i^2 = \left\langle \{\mathbf{r}_i(t+\Delta t) - \mathbf{r}_i(t)\}^2 \right\rangle, \quad (1)$$

where $\Delta t = 1$ ns. We assume that a water molecule is solid-like when δ_i^2 is smaller than 0.1 nm^2.[21,22] The maximum temperature at which more than half of water molecules in the brush region are solid-like is defined as the solidification temperature, T_s (see the supplementary material for more details).

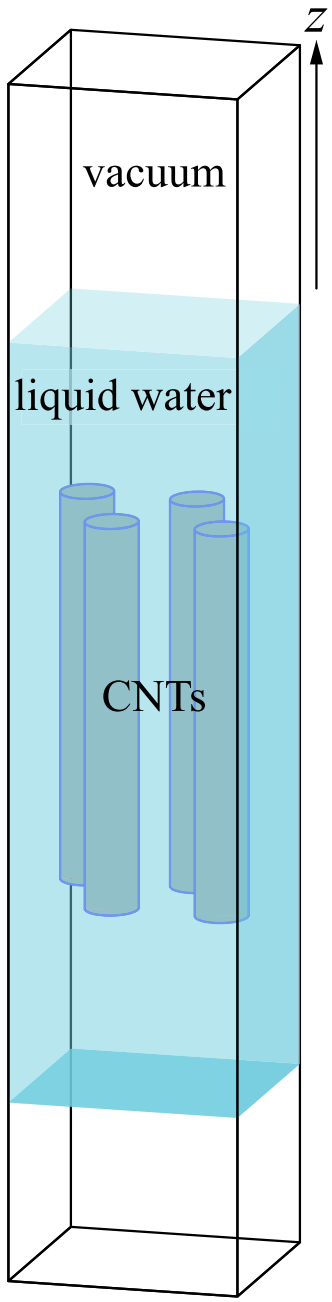

FIG. 1. Initial setup of the system.

RESULTS AND DISCUSSION

Figure 2 shows a side view and an axial projection of the ice structure in the brush region at T_s for armchair CNTs. Water molecules remain unfrozen during the simulation of 100 ns at the lowest temperature examined, 252 K, for CNTs that are larger than (10,10) in radius. The crystalline structure formed around (6,6) CNTs is remarkably ordered. This is the dtc structure found

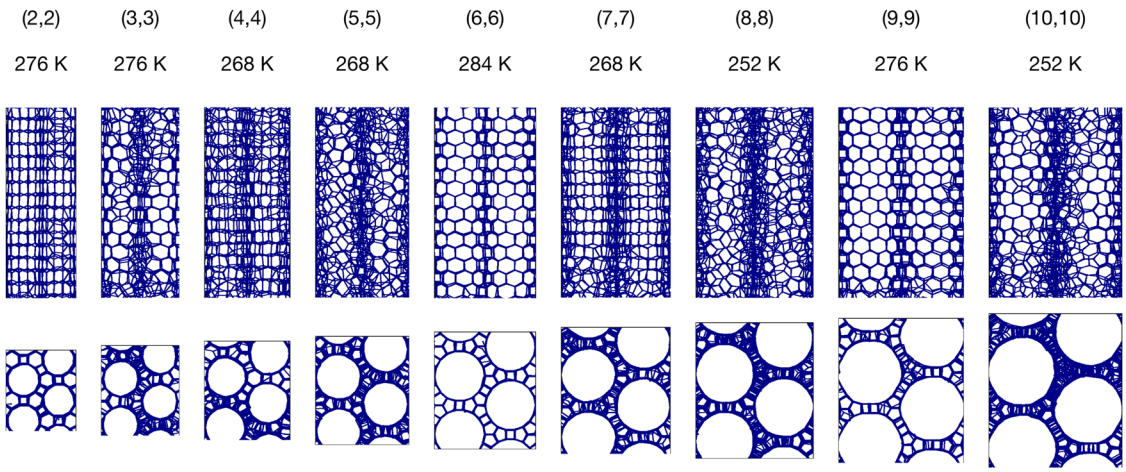

FIG. 2. Hydrogen bond network of water molecules in the brush region at T_s for nanobrushes of armchair CNTs.

in the previous study.[14] The structures around (2,2) and (9,9) CNTs are also highly ordered, but they are different from the dtc structure.

The ordered ice structures resemble those of CNTs made up with hexagons. The carbon atoms in CNTs are three-coordinated due to the sp^2 orbital, while water molecules prefer four-coordinated structures. Therefore, the water molecules in the first hydration shell of a CNT form a two-dimensional (2D) honeycomb structure with three hydrogen bonds, and the remaining one connects the layer of the first hydration shell and the layer of the second hydration shell. This is clearly seen in Fig. 3 that shows the hydrogen bonds in the two layers and the bonds connecting the layers in different colors. Water molecules located within 0.47 nm from the surface of CNTs are defined to be in the first layer, and other water molecules located within 0.75 nm are defined to be in the second layer. The black, red, and blue bonds in the top panels of Fig. 3 are the hydrogen bonds in the first layer, those in the second layer, and those connecting the two layers, respectively. Figure 3 helps to identify the new ice structures. We find that the ice structures in the nanobrush of (2,2) CNTs and (5,0) CNTs are topologically the same as zeolites AFI and CFI, respectively.[23] The ice structure in the nanobrush of (9,9) CNTs is the same as the dtc except the extended double-walled portion between adjacent channels. We call this structure xdtc. Structures of CNTs can be classified into several groups including zigzag and armchair types. Similarly, the cylindrical structures of the ice in the nanobrushes can be classified: AFI, dtc, and xdtc are zigzag type structures, while CFI is an armchair-like structure.

The relation between the CNT radius and the ice structure is summarized in Table I. As shown in Fig. 2, the hydrogen bond network in the brush region is not necessarily ordered even when water molecules become immobile at low temperatures. For example, there is no clear periodic order in the hydrogen bond network in the brush of (5,5) CNTs. Such structures are not listed in Table I.

Every structure listed in Table I can be decomposed into a small number of primitive blocks shown in Fig. 4. There are only six types of blocks. We call them h, r, s, t, u, and z. The colors of edges show possible connections between the primitive blocks. For example, a z-type block can share a blue or red edge with another z-type block or a t-type block, but it cannot share any edge with s, h, u, and r-type blocks. A channel structure can be represented by a sequence of primitive blocks. For example, $(hs)^6$ = hshshshshshs represents the AFI structure and $(ruuu)^2$ represents the CFI structure, as shown in Fig. 5. The six primitive blocks are classified into two groups. The h, s, t, and z-type primitive blocks have the same pitch along the z-direction. We call this group "Z" because the cylindrical layer must be a zigzag type for ice structures consisting of the primitive blocks included in this group. The primitive blocks of the other group, "A," are the r- and u-type blocks. They have a common pitch length along the z-direction that is different from the pitch of the Z group. The cylindrical layer structures of combinations of the A group blocks is an armchair type. The A group primitive blocks cannot coexist with the Z group primitive blocks in a crystal structure because of the difference in the pitch.

An interesting fact is that h^6 represents the structure of ice I_h. This means that it is possible to consider ice I_h as a zigzag type cylindrical structure. The chiral index of ice I_h is (3,0).

In Fig. 6(a), T_s is plotted against the radius of the CNTs. T_s decreases with increasing the radius except for the high T_s at 0.42 nm and at 0.60 nm due to the formation of the $(tz)^6$ and $(tzz)^6$ structures. It is expected that the $(tzzz)^6$ structure, referred to as "dtd" in the RCSR (Reticular Chemistry Structure Resource) database,[27] would show another peak. Formation of this structure may be observed in MD simulations when temperatures lower than the melting point of I_h, $T < 250$ K, are examined. The z, s, and r blocks, which appear between two CNTs, are made of squares, and therefore, the molecules in them are less stable than those in the t, u, or h block, which appear at the triple junction. As the diameter of the CNTs increases, the proportion of the former increases and the shape of the cylindrical cavity of ice becomes more hexagonal (see xdtc in Fig. 5). Consequently, the ice structure will become less stable and the CNTs are less wettable, and thus, T_s tends to be lower for larger radius. The range of T_s, as in Fig. 6(a), 252 K $\leqq T_s \leqq$ 288 K, is fairly wide, demonstrating that the thermodynamic stability of the crystal is sensitive to

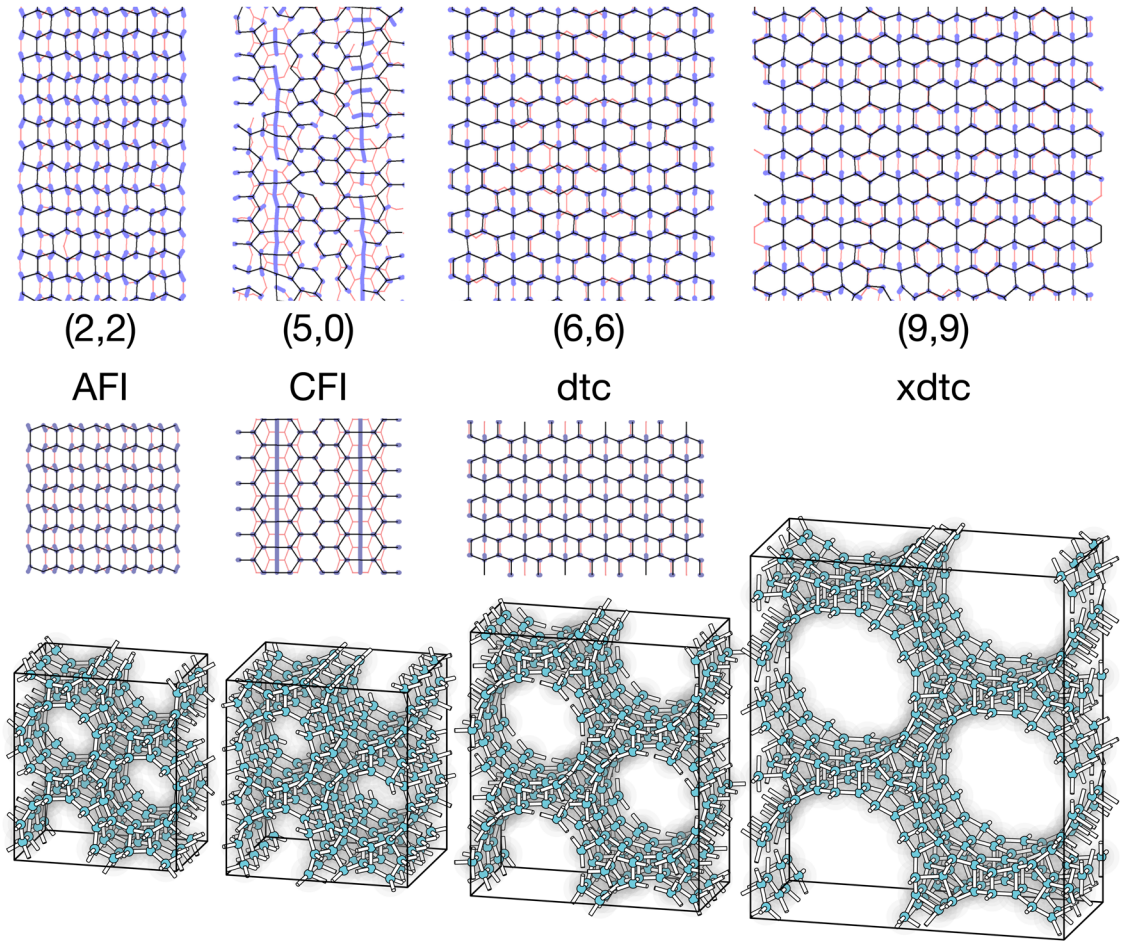

FIG. 3. Top panels: hydrogen bonds in the first shell of CNT (black), those in the second shell (red), and those connecting the two layers (blue) in the MD simulations at T_s. The horizontal axis and the vertical axis in the top panels correspond to the circumferential direction of the cylindrical structure and the *z*-axis of the simulation cell. Middle panels: networks of zeolites. Bottom panels: ideal crystalline structures. The ideal structures are generated by using the GenIce tool.[24]

TABLE I. Summary of ice structures found in the MD simulations of CNT nanobrushes in water.

CNT		Ice				
Chiral index	Radius (nm)	T_s (K)	Name	Symbol	Group	Chiral index
...	...	...	ice Ih	h^6	Z	(3,0)
(2,2)	0.14	280	AFI	$(hs)^6$	Z	(6,0)
(5,0)	0.20	272	CFI	$(ruuu)^2$	A	[a]
(6,0)	0.24	268		$(hstts)^2$	Z	(7,0)
(7,0)	0.28	268		$(hsts)^3$	Z	(8,0)
(10,0), (6,6)	0.39–0.43	288	dtc	$(tz)^6$	Z	(9,0)
(16,0), (9,9)	0.61–0.63	268	xdtc	$(tzz)^6$	Z	(12,0)
(12,12)	0.83	<252	(dtd)[b]	$(tzzz)^6$	Z	(15,0)

[a]The surface of the cylinder consists of various sizes of rings.
[b]Crystallization is not observed in the temperature range of the present work.

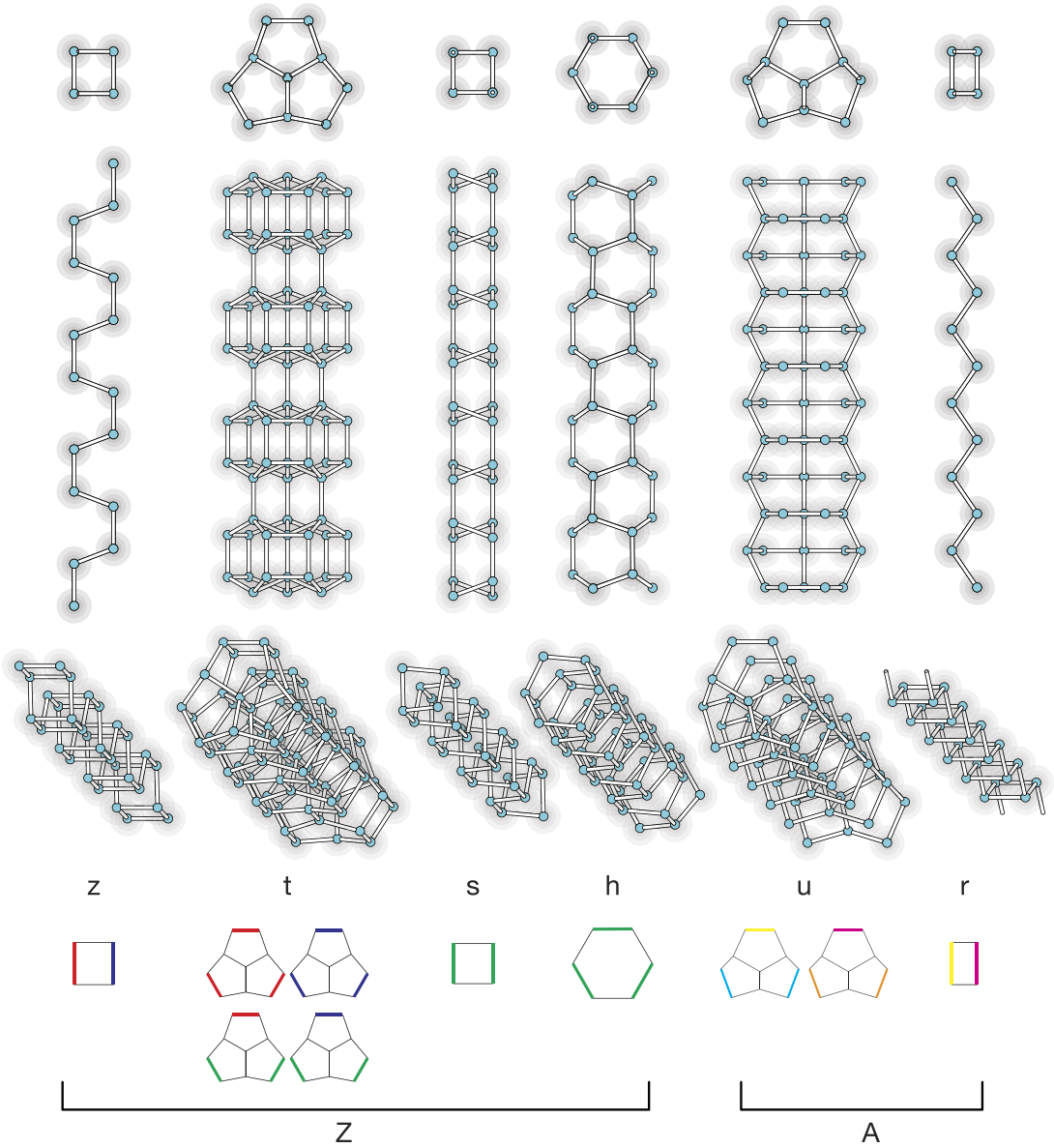

FIG. 4. Primitive structural blocks for the ice structures in CNT nanobrushes found in the MD simulations. The h block is also known as the hexagonal cage, which is one of the building blocks of ice I_h.[25,26]

the shape of confined space and the crystalline structure. Such results are observed for other systems.[28,29]

The deviation of the bond angles of the hydrogen-bonding network from the tetrahedral angle of 109.47° is evaluated using the tetrahedrality index, q, defined as[30]

$$q = 1 - \frac{3}{8}\sum_{j=1}^{4}\sum_{k=1}^{j-1}\left(\cos\psi_{jk} + \frac{1}{3}\right)^2, \tag{2}$$

where ψ_{jk} is the angle formed by the vectors connecting the oxygen atom of a given molecule and the oxygen atoms of its nearest neighbors j and k ($\leqq 4$). This index is unity when the four neighboring molecules are in a perfect tetrahedral configuration and zero on average when their positions are totally random. Figure 6(b) shows the dependence of the q-value on the CNT radius. There is a strong correlation between the q-value shown in (b) and T_s shown in (a) except for the CFI structure in the nanobrush of (5,0) CNT. This is probably because the ideal arrangement of the channels in the CFI structure is different from the regular triangular lattice. A fine adjustment of the positions of CNTs would result in higher T_s for this structure.

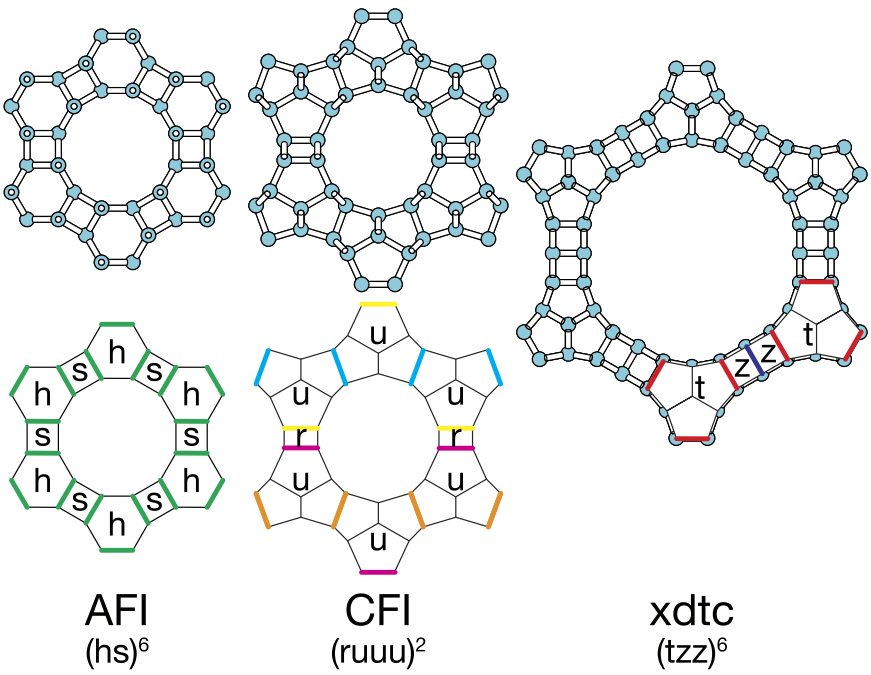

FIG. 5. AFI, CFI, and xdtc structures represented by the primitive blocks.

We compare the ice structure around armchair CNTs and that around zigzag CNTs at almost the same radius. The ice structure around (6,6) CNTs is the same as that around (10,0) CNTs (Table I). The ice structure around (9,9) CNTs is also the same as that around the corresponding zigzag (16,0) CNTs. The ice structure depends mainly on the diameter of the CNTs in nanobrushes. This can be related to the fact that the crystal structure of clathrate hydrate is mainly determined by the radius of the guest molecules and independent from the detailed shape of the guest molecules.[31] An exception is again the CFI structure. The CFI structure around (5,0) CNTs is different from the structure around (3,3) CNTs shown in Fig. 2. The surface structure of the channels of CFI is not a typical zigzag type made of flat hexagons but a more complicated structure. The present result indicates that there is a specific geometrical matching between the positions of carbon atoms on the surface of (5,0) CNTs and those of water molecules in the CFI structure.

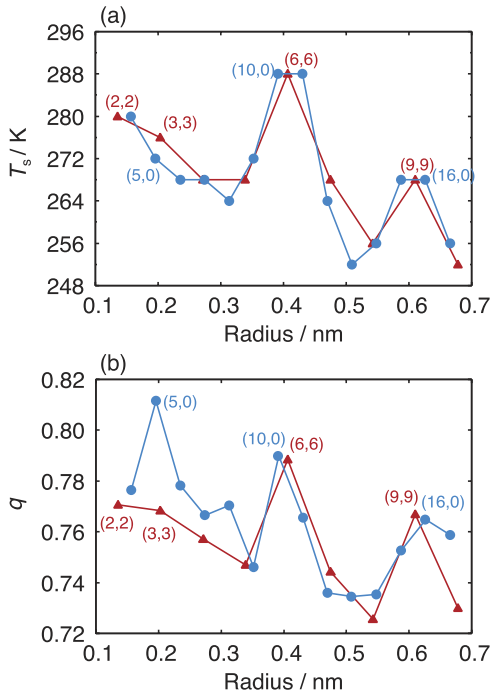

FIG. 6. (a) T_s plotted against the radius of CNTs for the nanobrushes of armchair CNTs (red) and zigzag CNTs (blue). The chiral index is shown for several CNTs. (b) Tetrahedrality index plotted against the radius of CNTs.

One may think that an ice structure with large cylinders can be formed with CNTs that are smaller than the corresponding CNTs for the ice structure when the spacing between the CNTs is larger than 0.94 nm. We consider whether dtc forms with (2,2) CNTs instead of (6,6) CNTs as an example. The distance between a carbon atom in a (6,6) CNT and the closest oxygen atom in the dtc structure corresponds to the minimum position of the van der Waals (vdW) interaction. The radius of the (2,2) CNT is smaller than that of the (6,6) CNT by 0.27 nm. If (6,6) CNTs in dtc are replaced with (2,2) CNTs, the vdW interaction becomes almost zero. As shown in Fig. 5 of Paper I,[14] the chemical potential of dtc cannot be lower than that of liquid water without the CNT-water attractive vdW interactions at temperatures higher than 250 K. Therefore, the dtc structure cannot form with the (2,2) CNT. The difference in radius between the (5,5) CNT and (6,6) CNT is only 0.07 nm. Thus, the change in the vdW interactions caused by replacement of (6,6) CNTs in dtc with (5,5) CNTs is expected to be small. The dtc structure may form with (5,5) CNT when the gap distance between the surfaces of CNTs is close to 0.94 + 0.07 × 2 = 1.08 nm and the temperature is low enough.

SUMMARY

We have investigated crystalline structures of water around CNTs in nanobrushes using MD simulations. The CNTs are located in a regular triangular arrangement, and the distance between the surfaces of CNTs is fixed to 0.94 nm, which is the best spacing for the bilayer structure of water. The range of the radius of the CNTs is $0.12 < R < 2.2$ nm. Several stable porous ice structures spontaneously form in the MD simulations even at temperatures higher than the melting temperature of ice I_h when the radius of CNTs matches with the size of the cavities of the ice structure. We have proposed a protocol to classify the porous ice crystals on the basis of the fact that all of them can be decomposed into a small number of structural blocks. The crystallization temperature suggests that the dtc structure, or the $(tz)^6$ structure, is thermodynamically most stable among the crystals observed in this study. The hydrogen bond network of the CFI structure is less distorted than the dtc structure although the crystallization temperature is lower for CFI. It might be possible to make the crystallization temperature of CFI higher than that of dtc by adjusting the positions of CNTs in the brush. There might be arrangements of CNTs that facilitate formation of quite stable ice structures other than the 2D triangular lattice. Such brushes may be useful for energy storage and separation processes utilizing the phase transition of water.

SUPPLEMENTARY MATERIAL

The supplementary material consists of one section and four figures and describes how to determine the temperature at which water solidifies in the nanobrushes.

ACKNOWLEDGMENTS

This work was supported by JSPS KAKENHI Grant No. 20H05272, and the Research Center for Computational Science provided computational resources.

DATA AVAILABILITY

The data that support the findings of this study are available from the corresponding author upon reasonable request.

REFERENCES

[1] A. Pohorille and L. R. Pratt, Origins Life Evol. Biospheres **42**, 405 (2012).
[2] G. A. Jeffrey, J. Inclusion Phenom. **1**, 211 (1984).
[3] H. Tanaka, T. Yagasaki, and M. Matsumoto, Planet. Sci. J. **1**, 80 (2020).
[4] P. Linga, R. Kumar, and P. Englezos, J. Hazard. Mater. **149**, 625 (2007).
[5] T. Sugahara, H. Machida, S. Muromachi, and N. Tenma, Int. J. Refrig. **106**, 113 (2019).
[6] A. Falenty, T. C. Hansen, and W. F. Kuhs, Nature **516**, 231 (2014).
[7] L. Del Rosso, M. Celli, and L. Ulivi, Nat. Commun. **7**, 13394 (2016).
[8] M. M. Conde, C. Vega, G. A. Tribello, and B. Slater, J. Chem. Phys. **131**, 034510 (2009).
[9] G. A. Tribello, B. Slater, M. A. Zwijnenburg, and R. G. Bell, Phys. Chem. Chem. Phys. **12**, 8597 (2010).
[10] Y. Huang, C. Zhu, L. Wang, X. Cao, Y. Su, X. Jiang, S. Meng, J. Zhao, and X. C. Zeng, Sci. Adv. **2**, e1501010 (2016).
[11] E. A. Engel, A. Anelli, M. Ceriotti, C. J. Pickard, and R. J. Needs, Nat. Commun. **9**, 2173 (2018).
[12] Y. Liu and L. Ojamäe, Phys. Chem. Chem. Phys. **20**, 8333 (2018).
[13] T. Matsui, M. Hirata, T. Yagasaki, M. Matsumoto, and H. Tanaka, J. Chem. Phys. **147**, 091101 (2017).
[14] T. Yagasaki, M. Yamasaki, M. Matsumoto, and H. Tanaka, J. Chem. Phys. **151**, 064702 (2019).
[15] B. Hess, C. Kutzner, D. van der Spoel, and E. Lindahl, J. Chem. Theory Comput. **4**, 435 (2008).
[16] W. L. Jorgensen, D. S. Maxwell, and J. Tirado-Rives, J. Am. Chem. Soc. **118**, 11225 (1996).
[17] G. A. Kaminski, R. A. Friesner, J. Tirado-Rives, and W. L. Jorgensen, J. Phys. Chem. B **105**, 6474 (2001).
[18] Q. Zhao and J. Zhang, Small **10**, 4586 (2014).
[19] X. Zhao, Y. Liu, S. Inoue, T. Suzuki, R. O. Jones, and Y. Ando, Phys. Rev. Lett. **92**, 125502 (2004).
[20] J. L. F. Abascal and C. Vega, J. Chem. Phys. **123**, 234505 (2005).
[21] J. Vatamanu and P. G. Kusalik, J. Chem. Phys. **126**, 124703 (2007).
[22] T. Yagasaki, M. Matsumoto, and H. Tanaka, J. Phys. Chem. B **122**, 3396 (2018).
[23] C. Baerlocher and L. B. McCusker, http://www.iza-Structure.org/databases/, 2008.
[24] M. Matsumoto, T. Yagasaki, and H. Tanaka, J. Comput. Chem. **39**, 61 (2018).
[25] M. Matsumoto, T. Yagasaki, and H. Tanaka, Phys. Rev. Lett. **115**, 197801 (2015).
[26] A. Haji-Akbari and P. G. Debenedetti, Proc. Natl. Acad. Sci. U. S. A. **112**, 10582 (2015).
[27] M. O'Keeffe, M. A. Peskov, S. J. Ramsden, and O. M. Yaghi, Acc. Chem. Res. **41**, 1782 (2008).
[28] T. James, D. J. Wales, and J. Hernández-Rojas, Chem. Phys. Lett. **415**, 302 (2005).
[29] H. Tanaka and K. Koga, J. Chem. Phys. **123**, 094706 (2005).
[30] J. R. Errington and P. G. Debenedetti, Nature **409**, 318 (2001).
[31] M. v. Stackelberg, Naturwissenschaften **36**, 327 (1949).